INT. J. NUM. METH. HEAT FLUID FLOW, VOL. 5, 577–588 (1995)

MODELLING DUMP COMBUSTOR FLOWS WITH AND WITHOUT SWIRL AT THE INLET USING REYNOLDS STRESS MODELS

J. H. TSAI, C. A. LIN AND C. M. LU

Department of Power Mechanical Engineering, National Tsing Hua University, Hsinchu, Taiwan 30043

ABSTRACT

Numerical simulations were applied to suddenly-expanding-pipe flows, with and without swirl at the inlet, using an eddy-viscosity type k–ε model and Reynolds stress transport model variants. The predicted mean and turbulence results were compared with measurements. For the non-swirling case, the flowfield was well represented by all the models, though the k–ε predictions showed a slightly higher level of radial diffusive transport across the shear layer in the recirculation zone. As for the weakly swirling case, while all models, especially the stress models, give accurate values of the mean flow and turbulence fields in regions remote from the central vortex core; the biggest discrepancies between predictions and measurements occurred along the centreline in which all the models failed to reproduce correctly the strength of the decay of swirl-induced deceleration of the axial velocity. The intensity of the turbulence along the centreline was also severely underpredicted by all the models and this contributed to the misrepresentations of the shear stresses and, hence, the mean flow development predicted by the stress models.

KEY WORDS Dump combustor k–ε model Reynolds stress Recirculation

INTRODUCTION

Recirculation and jet injection through axisymmetric expansions are of considerable interest to engineers because of their frequent occurrence in industrial applications. In air breathing systems, for example, the basic geometry of the ramjet combustor is a sudden expansion dump combustor. A confined jet exits into a sudden expansion within which reverse flow occurs immediately downstream of the sudden expansion. The corner recirculation zone is used to enhance flame stability and, therefore, the size of the recirculation zone influences the performance of the combustor. Other factors such as the mixing between the fuel and the heat is likely also to exert a significant influence on combustion efficiency.

Swirling motion accompanying the incoming confined jet is often employed as a mechanism to further promote or control mixing between the fuel spray jet and the adjacent air and, in some instances, to stabilise the combustion zone due to the presence of the swirl-induced central recirculation region. From a theoretical point of view, a 'two-dimensional' swirling flow is considerably more complicated than two-dimensional plane flows, since additional strains arise due to the azimuthal motion requiring the solution for azimuthal momentum and, hence, the swirl related stresses, if a stress model were employed, for $\overline{w^2}$, $\overline{uw}$ and $\overline{vw}$. Indeed, the strain field may be said to be virtually as complex as any three-dimensional flow. Swirl introduces intense

0961–5539/95/070577–12$2.00

Received September 1993
Revised May 1994

azimuthal streamline curvature and hence curvature-turbulence interaction affects all six independent stress components.

Numerous numerical studies have been made by various researchers to study the effects of swirl and in a variety of combustor geometries. These include free jets[1,2] and confined jets with and without vortex breakdown[3–7]. The studies demonstrate that the superiority of stress closures over the k–ε model in the prediction of swirling flows, though the merits of various stress model variants differ at different swirl levels. For strongly swirling flows, for example, the superiority of the stress model[5,6] is reflected primariy by the lower level of shear stresses due to the proper representation of the interaction between swirl-induced curvature and stresses. In most confined swirling flows, however, due to the lack of complete experimental data, no measured shear stresses were available for comparisons to gain further insights of the turbulent transport processes.

The present research aims at the predicting capability of various turbulence models on sudden-expanding-pipe geometry flows with the emphasis of the influences of the inlet swirl level on the flowfield pattern. A non-swirling inlet and a weakly swirling inlet with swirl number of 0.3 form the basis of the investigations. For the weakly swirling case, the decay of swirling motion causes strong streamline variation of pressure, and, consequently, leads to a deceleration of its central vortex core, but it is not sufficient to cause a vortex breakdown. Detailed comparisons of the predicted results and measurements will be presented with special emphasis on the effects of turbulence quantities on the mean flow-field.

THE COMPUTATIONAL APPROACH

The governing equations

The behaviour of the flow is in general governed by the fundamental principles of classical mechanics expressing the conservation of mass and momentum. The time-averaged equations for high-Reynolds-number flow, may be described by the equations (in terms of cartesian tensors):

$$\frac{\partial(\rho U_i)}{\partial x_i}=0 \tag{1}$$

$$\frac{\partial(\rho U_i U_j)}{\partial x_j}=-\frac{\partial P}{\partial x_i}+\frac{\partial}{\partial x_i}\left[\mu_l\left(\frac{\partial U_i}{\partial x_j}+\frac{\partial U_j}{\partial x_i}\right)-\rho\overline{u_i u_j}\right] \tag{2}$$

where $\overline{u_i u_j}$ is turbulent flux arising from the time-averaging process.

In the present application, turbulence is described either by the high-Reynolds-number $k-\varepsilon$ eddy-viscosity model of Jones and Launder[8]*, used here merely as a datum closure, or by high-Reynolds-number Reynolds-stress closure, as detailed below, all involving six equations for the independent stresses $\overline{u_i u_j}$ and a seventh equation for the isotropic turbulence-energy dissipation ε. Suffice it to confine attention here to the Cartesan framework described in terms of tensor notation.

The Reynolds stress closure will be expressed in a general form, and this may be written as:

$$\frac{\partial}{\partial x_k}(\rho U_k \overline{u_i u_j})=d_{ij}+P_{ij}-\varepsilon_{ij}+\phi_{ij} \tag{3}$$

in which d_{ij} represents diffusion and is approximated by the simplified gradient-diffusion model,

$$d_{ij}=\frac{\partial}{\partial x_k}\left[\frac{\mu_t}{\sigma_k}\frac{\partial \overline{u_i u_j}}{\partial x_k}\right] \tag{4}$$

*This model does not account for the curvature effect through a curvature Richardson number.

Table 1

C_μ	C_1	C_2	C'_{1w}	C'_{2w}	σ_k	σ_ε	$C_{\varepsilon 1}$	$C_{\varepsilon 2}$
0.09	1.8	0.6	0.5	0.3	1.0	1.3	1.44	1.92

P_{ij} stands for the (exact) stress generation resulting from the interaction between stresses and strains,

$$P_{ij} = -\rho\overline{u_i u_k}\frac{\partial U_j}{\partial x_k} - \rho\overline{u_j u_k}\frac{\partial U_i}{\partial x_k} \tag{5}$$

and $2/3\rho\delta_{ij}\varepsilon$ models stress dissipation, ε_{ij}, on the assumption that this process is isotropic and may thus be characterised by the dissipation of turbulence energy, ε. The term ϕ_{ij} identifies pressure/strain interaction and consists of three model components, representing, respectively, 'return to isotropy', 'isotropisation of mean-strain and turbulence correlation' and 'redistributive effects arising from wall reflection of pressure fluctuations'.

The stress model closure variant (IPGL) adopted here is that of Gibson & Launder[9], which may be written as:

$$\phi_{ij1} = -C_1\rho\frac{\varepsilon}{k}\left[\overline{u_i u_j} - \frac{\delta_{ij}}{3}\overline{u_k u_k}\right] \tag{6}$$

$$\phi_{ij2} = -C_2\left[P_{ij} - \frac{\delta_{ij}}{3}P_{kk}\right] \tag{7}$$

$$\phi_{ijw1} = C'_{1w}\rho\frac{\varepsilon}{k}\left[\overline{u_k u_m}n_k n_m\delta_{ij} - \frac{3}{2}\overline{u_k u_i}n_k n_j - \frac{3}{2}\overline{u_k u_j}n_k n_i\right]f \tag{8}$$

$$\phi_{ijw2} = C'_{2w}\left[\phi_{km2}n_k n_m\delta_{ij} - \frac{3}{2}\phi_{ik2}n_k n_j - \frac{3}{2}\phi_{jk2}n_k n_i\right]f \tag{9}$$

where n_i is the wall-normal unit vector in the direction i and $f = C_\mu^{0.75}k^{1.5}/(\varepsilon\kappa y)$ with y being the distance to the closest wall, taken along the co-ordinate line normal to the wall.

The rate of turbulence-energy dissipation, ε, appearing in the stress equations is determined from its own transport equation which takes the form,

$$\frac{\partial}{\partial x_k}(\rho U_k\varepsilon) = \frac{\partial}{\partial x_k}\left[\frac{\mu_t}{\sigma_\varepsilon}\frac{\partial\varepsilon}{\partial x_k}\right] + C_{\varepsilon 1}\frac{\varepsilon}{k}P_{kk}/2 - C_{\varepsilon 2}\rho\frac{\varepsilon^2}{k} \tag{10}$$

The constants appearing in the above turbulence-model equations are as listed in *Table 1.*

A variant of the above closure (IPCM), proposed by Fu *et al.*[4], includes the convection tensor C_{ij} in ϕ_{ij2} to arrive at the co-ordinate invariant, 'objective' model form,

$$\phi_{ij,2} = -C_2[P_{ij} - C_{ij} - 1/3\delta_{ij}(P_{kk} - C_{kk})] \tag{11}$$

The second variant (IPGY), proposed by Gibson and Younis[2], modifies the coefficients C_1 and C_2 by taking the values of 3.0 and 0.3, respectively.

Numerical algorithm

The above closures have been incorporated into a curved-orthogonal finite-volume procedure designed for the solution of general three-dimensional, time-dependent, recirculating flows[10]. This scheme solves discretised versions of all equations on a staggered finite-volume arrangement. A staggered storage is adopted not only for the velocity components but also for the shear stresses, shown in *Figure 1*,—an arrangement which aids stability by ensuring a strong numerical

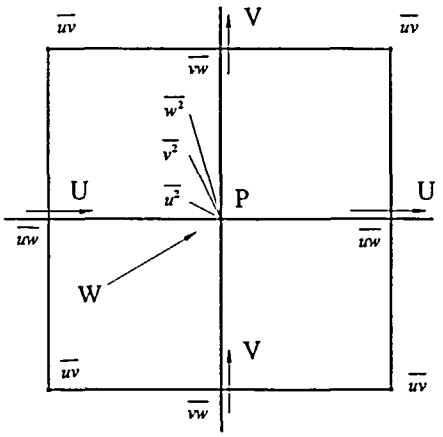

Figure 1 Staggered arrangement of the control volume

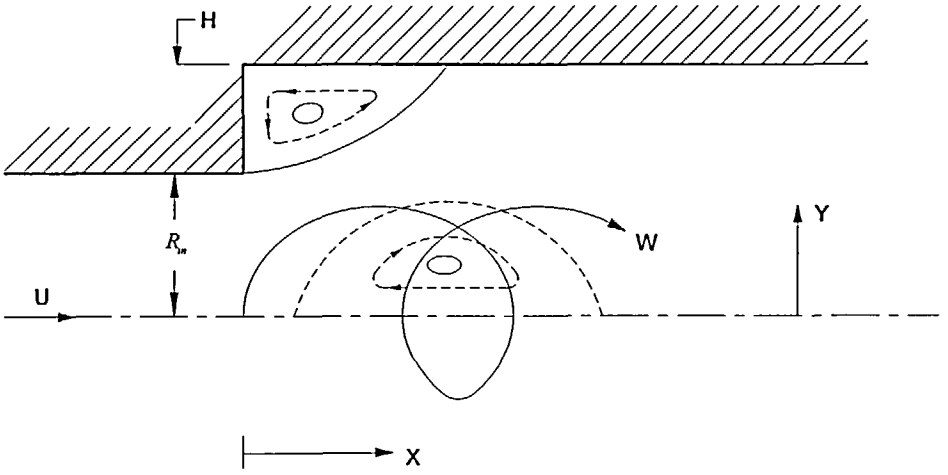

Figure 2 Geometry of the sudden-expanding pipe

coupling between stresses and primary strains. The principle of mass-flux continuity is imposed indirectly via the solution of pressure-correction equations according to the SIMPLE[11] algorithm. The flow-property values at the volume faces contained in the convective fluxes which arise from the finite-volume integration process are approximated by the quadratic upstream-weighted interpolation scheme QUICK[12]. Though the present case is a steady state solution, it was found that using a time marching process will enhance stability, especially when stress models are employed. The solution process consists of a sequential algorithm in which each of the eleven sets of equations in linearised form, is solved separately by application of an alternate-direction tri- or penta-diagonal line-implicit solver.

Convergence was judged by monitoring the magnitude of the absolute residual sources of mass and momentum, normalised by the respective inlet fluxes. The solution was taken as having converged when all above residuals fell below 0.5%.

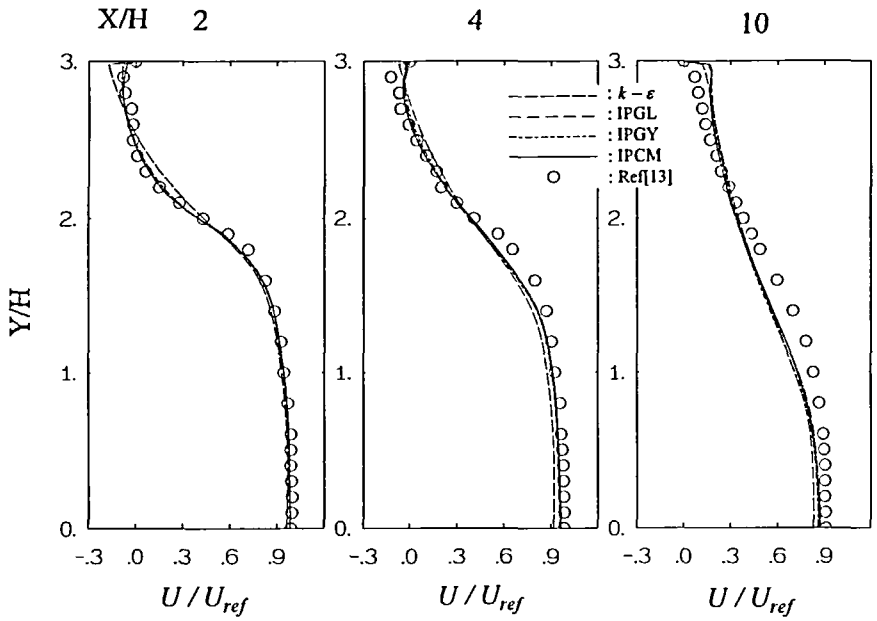

Figure 3 Axial velocity distribution (Swirl no.=0)

GEOMETRY AND BOUNDARY CONDITIONS

The geometry of the dump combustor is shown in *Figure 2*. The pipe expansion ratio and the swirl number are 1.5 and 0.3, respectively. The inlet velocity is known to be 19.2 m/s, corresponding to a Reynolds number of 1.25×10^5 based on the inlet pipe diameter, while its turbulence quantities were taken from the experiment of Favaloro *et al.*[13]. Experimental data are available from 0.38 step heights downstream the sudden expansion at which point the numerical simulation starts. The numerical mesh, of size 80×40, is non-uniform both in the x and y directions. The level of turbulence dissipation was obtained by using $\varepsilon_{in} = k_{in}^{1.5}/L$ where L was chosen to be $0.5\, R_{in}$[7].

At the wall, the tangential velocity component U was assumed to vary logarithmically between the semi-viscous sublayer, at $y_v^+ = 11.2$, and the first computational node lying in the region $30 < y^+ < 100$. This treatment yielded boundary conditions for the shear stresses and also permitted the volume-averaged near-wall generation rates of the tangential normal stresses to be computed over the associated near-wall finite volumes (the level of the wall-normal intensity was assumed negligibly small). The linear variation of the turbulent length scale, $L = \kappa y/C_\mu^{3/4}$, in the log-law region, together with $\varepsilon = k^{3/2}/L$, and the invariant value $\varepsilon = 2\mu_l k_v/(\rho y_v^2)$ in the viscous sublayer, allowed the volume-averaged dissipation rate to be determined; details may be found in Reference 14. This same L-variation was also used to prescribe explicitly the dissipation rate at the near-wall cpmputational node, serving as the boundary condition for inner-field cells.

RESULTS AND DISCUSSIONS

The flow field can be characterised by two distinct regions. The first is the corner recirculation zone caused by the sudden expansion of the pipe and the second is, for the swirling case, the decay of swirl-induced deceleration of the centre vortex core manifested itself by the appearance of a trough in the axial velocity profiles along the pipe axis. Both processes involve strong streamline curvature, therefore diffusive processes, physical or numerical, were influential. Initial

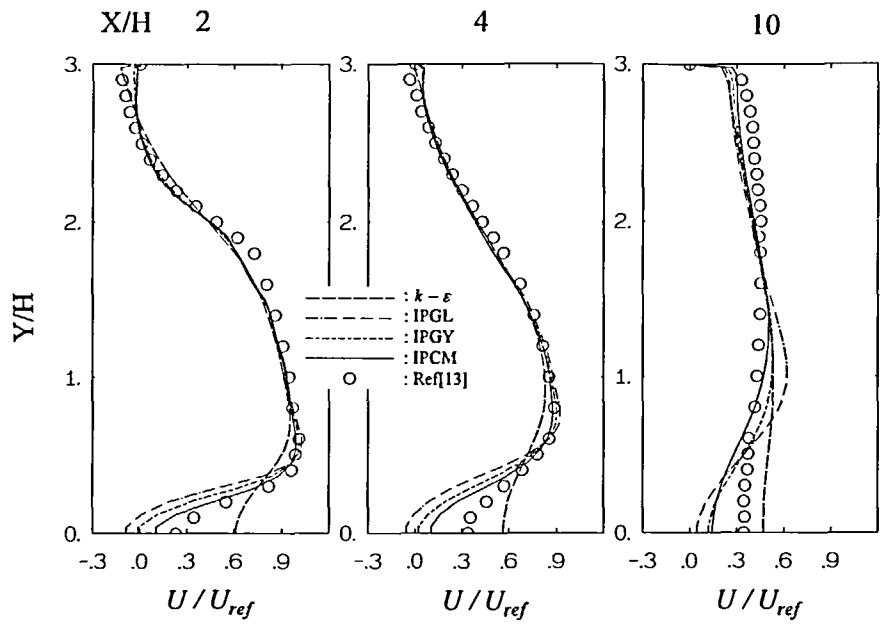

Figure 4 Axial velocity distribution (Swirl no. = 0.3)

tests on the influences of the convection scheme revealed that the differences between the second order QUICK and the first order hybrid scheme was negligibly small. Therefore, the mesh employed will be deemed to be satisfactory and further refinements of the mesh will not be beneficial.

Influences of the turbulence models on the predicted flowfield can be best exemplified by observing the axial velocity profiles, *Figures 3* and *4*, at several selected locations. For the non-swirling case, the flowfield was well represented by all the models, though the $k-\varepsilon$ results showed a relatively higher level of diffusive transport in the recirculation region. As for the weakly swirling case, shown in *Figure 4*, it is observed that, while all the models predicted similar axial development in regions beyond the central vortex core, the biggest discrepancies between predictions and measurements occurred along the centreline; the $k-\varepsilon$ model predicted a faster axial velocity recovery and a too slow axial velocity development was returned by the stress models. These imply that a too weak and a too strong centreline axial velocity deceleration due to the presence of decay of swirl-induced adverse pressure gradients, were predicted by the $k-\varepsilon$ model and stress models, respectively. Among the stress models, the IPCM exhibited a relatively better centreline development. The reduction of the strength of the corner recirculation zone due to the presence of swirl can also be observed in *Figures 3* and *4* at locations X/H = 4 and 10.

Referring to the swirl velocity, as shown in *Figure 5*, it is clearly identified that $k-\varepsilon$ model exhibited a slightly higher level of diffusive transport, at X/H = 2, in the centre core region; however, at X/H = 10, the computed results had manifested themselves, in accord with the measurements, by a return to the solid body rotation profiles. In contrast, the stress model simulations showed a relatively reduced level of radial transport. The retardation of turbulence transport persisted further downstream and was, however, contrary to what was reflected by the measurements.

It should be pointed out that Lin and Tsai[7] computed the same flow but with a higher swirl number, S = 0.5, and the results indicated that the stress models predicted well the development

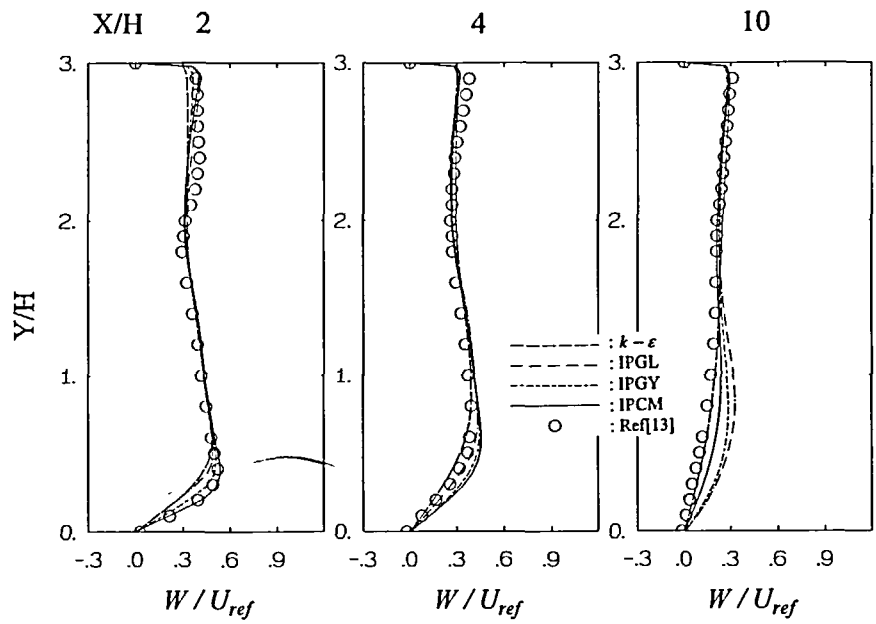

Figure 5 Swirl velocity distribution (Swirl no.=0.3)

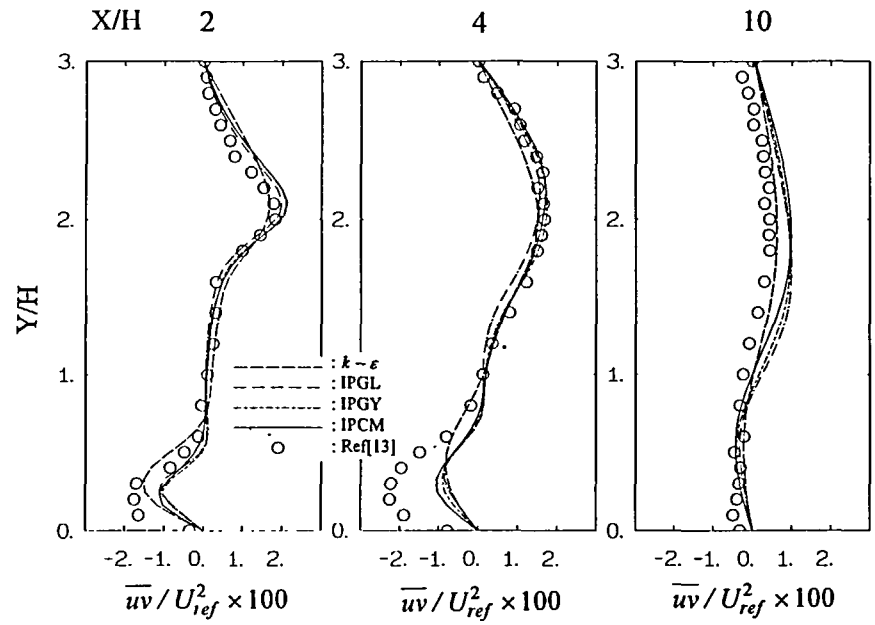

Figure 6 Shear stress $\overline{uv}$ distribution (Swirl no.=0.3)

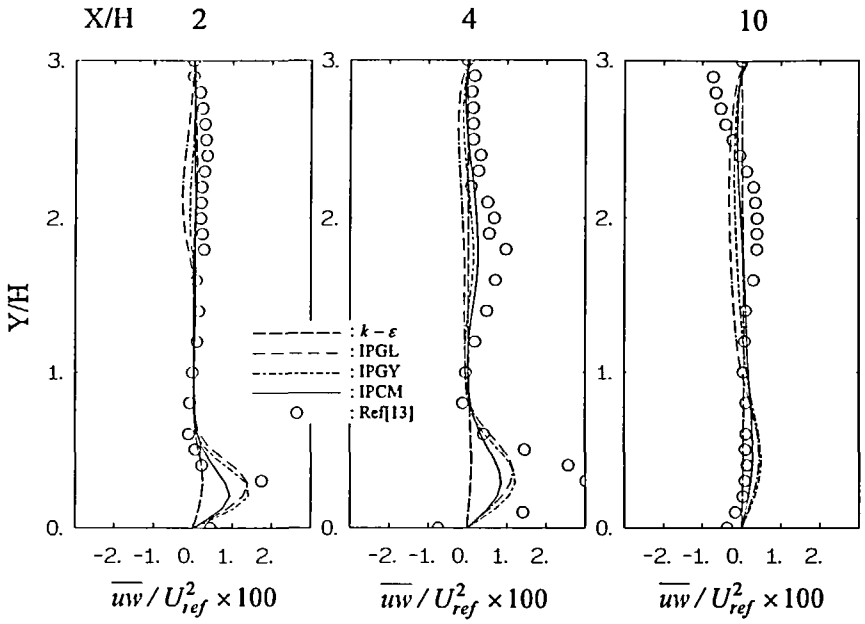

Figure 7 Shear stress $\overline{uw}$ distribution (Swirl no. = 0.3)

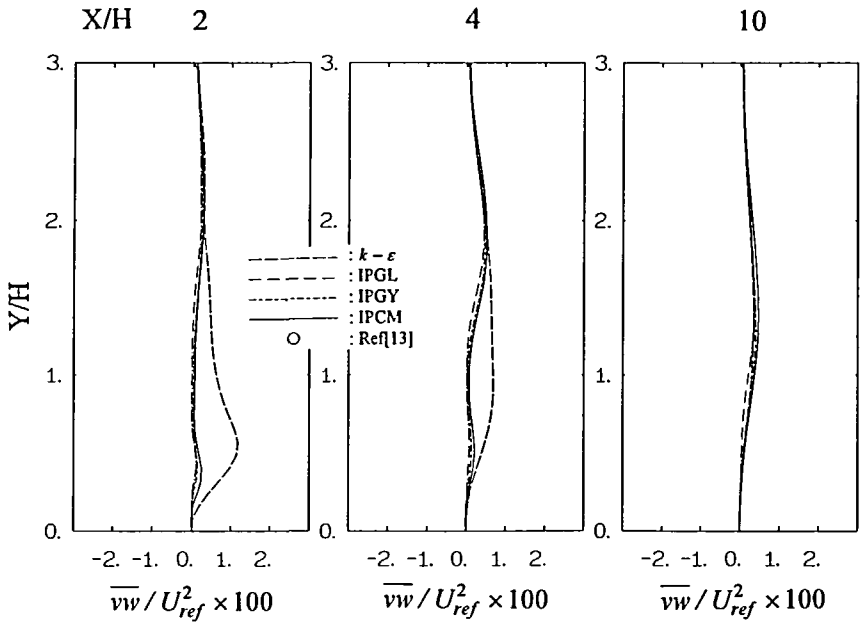

Figure 8 Shear stress $\overline{vw}$ distribution (Swirl no. = 0.3)

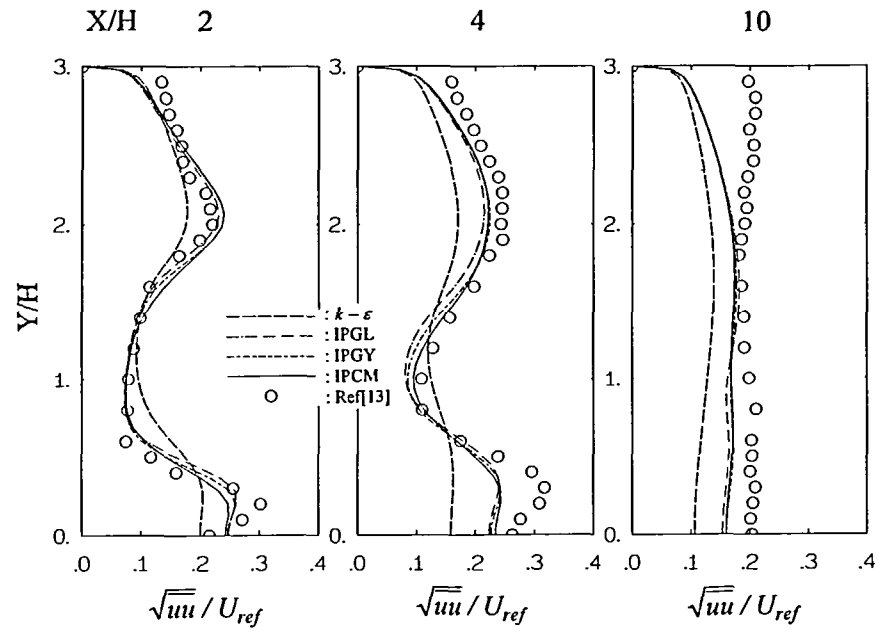

Figure 9 Turbulence intensity $\sqrt{\overline{uu}}$ distributions (Swirl no.=0.3)

of the centreline axial velocity, especially the strength of the decay of swirl-induced centreline recirculation zone. In contrast, the $k-\varepsilon$ model showed a faster recovery of the axial velocity along the centreline region, indicating a more intense radial transport at this region. This predicted retardation of radial transport by the stress models was consistent in both the S=0.3 and S=0.5 cases, albeit stress model predictions did not respond correctly to the reduction of the strength of the swirling motion.

Attention will be directed here to the turbulence quantities which act as the source term in the mean flow equations. Since the non-swirling case was fairly well predicted by the models, emphasis will be focused on the swirling case only. *Figures 6–8* show comparisons of the shear stresses distributions. The higher level of shear stress $\overline{uv}$ predicted by the $k-\varepsilon$ model, shown in *Figure 6*, at X/H=2, in the centreline region explains the more diffusive nature of the axial velocity predicted by the eddy-viscosity model. The stress model, however, indicated an overdamped $\overline{uv}$ profiles in accordance with the mean flow predictions, though the predictions by IPCM was marginally bettern among the stress models. The more diffusive nature of the swirl velocity predicted by $k-\varepsilon$ model is brought out more clearly by the $\overline{vw}$ distributions. By reference to *Figures 6* and *7*, it is also apparent that the biggest discrepancies between the predictions and measurements occur in the centre core regions at locations X/H=2 and 4.

The comparisons of the normal stress profiles which affect the shear stresses through their generation processes, are shown in *Figures 9–11*. While the $k-\varepsilon$ model predicted a fairly isotropic stress field, the stress models indicate a higher level of anisotropy of the normal stress fields. The measurements show, however, two distinct features. Beyond Y/H=0.5, the measured stress field is more anisotropic and was well represented by the stress models. The second is the central core region where extensive mixing seemed to have taken place and the measurements exhibited a more isotropic stress field. On the other hand, the stress models still predicted a higher level of anisotropy indicating that the pressure-strain models were in fact inadequate. All the models underpredicted $\overline{v^2}$ and $\overline{w^2}$ along the centreline. This underprediction of the normal stresses in

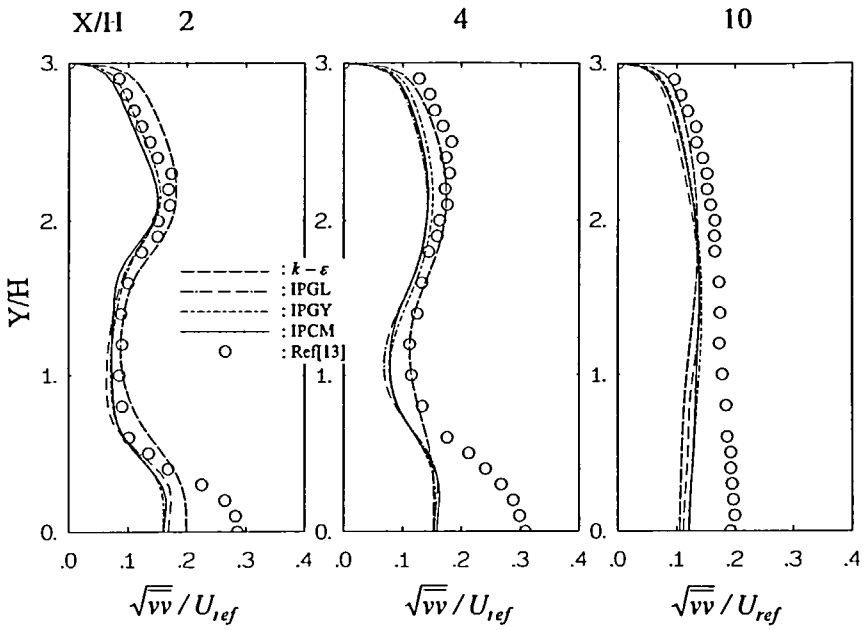

Figure 10 Turbulence intensity $\sqrt{\bar{v}\bar{v}}$ distributions (Swirl no. = 0.3)

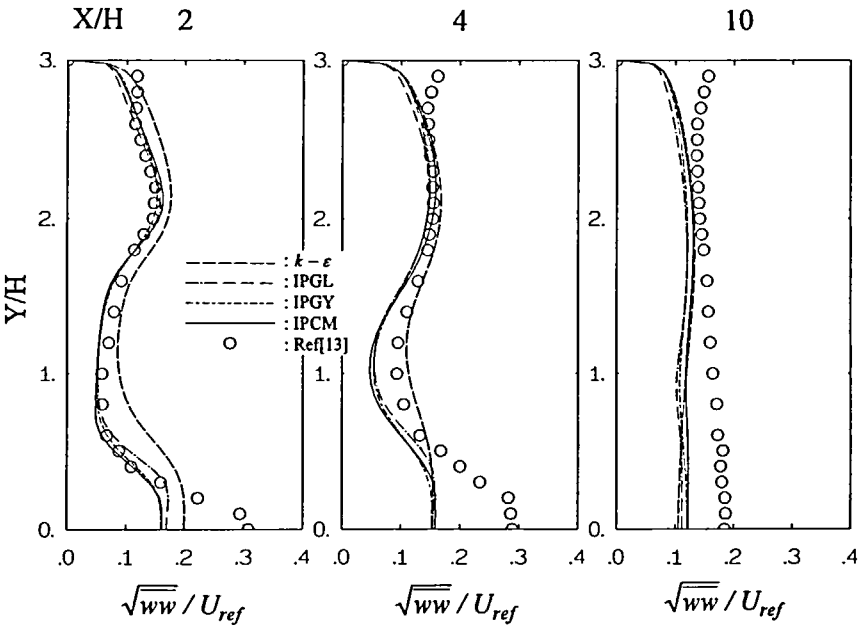

Figure 11 Turbulence intensity $\sqrt{\bar{w}\bar{w}}$ distributions (Swirl no. = 0.3)

this region resulted in the low level of shear stresses, $\overline{uv}$, $\overline{uw}$ predicted by stress models, as was observed earlier. The smaller level of $\overline{v^2}$ predicted by the stress models in the centreline region was the cause of the model predictions of slower recovery of the axial velocity, as was indicated by the overdamped level of the $\overline{uv}$ profiles.

CONCLUSIONS

Computational studies were applied to sudden-expanding-pipe flows, with and without swirl at the inlet, by eddy-viscosity type $k-\varepsilon$ model and Reynolds stress transport model variants. The predicted results indicated that, for the non-swirling case, the flowfield was well represented by all the models, though the $k-\varepsilon$ predictions showed a slightly higher level of radial diffusive transport across the shear layer in the recirculation zone. As for the weakly swirling case, while all models, especially the stress models, predicted well the mean and turbulence fields in regions remote from the central vortex core, the biggest discrepancies between predictions and measurements occurred along the centreline. In this region, all the models failed to correctly reproduce the strength of the decay of swirl-induced deceleration of the central vortex core, with a too strong and a too weak axial centreline axial velocity recovery predicted by the $k-\varepsilon$ model and the stress models, respectively. The intensity of the turbulence was also severely underpredicted by all the models along the centreline and this underprediction of the normal stresses was the cause of the slower development of the axial and swirl velocities predicted by the stress models. Among the stress models, the IPCM variant performed marginally better.

ACKNOWLEDGEMENTS

This research work was supported by the National Science Council of Taiwan under grant NSC-82-0401-E-007-251 and the computational facilities were provided by the National Centre for High-Performance Computing of Taiwan which the authors gratefully acknowlege. The authors also wish to express gratitude for the experimental data in diskette form provided by Dr Ahmed.

REFERENCES

1 Launder, B. E. and Morse, A. P. Numerical prediction of axisymmetric free shear flow with Reynolds stress closure, *Turbulent Shear Flow I* (Eds Durst, F., Launder, B. E., Schmidt, F. W. and Whitelaw, J. H.), 279–294, Springer-Verlag (1979)

2 Gibson, M. M. and Younis, B. A. Calculation of swirling jet with a Reynolds stress closure, *Physics of Fluids*, 29, 38–48 (1986)

3 Weber, R., Boysan, F., Swithenbank, J. and Roberts, P.A. Computations of near field aerodynamics of swirling expanding flows, *21st Int. Symp. on Combustion/The Combustion Institute*, 1435–1443 (1986)

4 Fu, S., Launder, B. E. and Leschziner, M. A. Modelling strongly swirling recirculating jet with Reynolds-stress transport closure, *Pro . 6th Symp. on Turbulent Shear Flows*, Toulose, 17.6.1-17.6.6 (1987)

5 Hogg, S. and Leschziner, M. A. Computation of Highly Swirling Confined Flow with a Reynolds stress turbulence model, *AIAA J.*, **27**, 53–63 (1989)

6 Jones, W. P. and Pascau, A. Calculation of confined swirling flows with a second moment closure, *Trans. ASME J. of Fluids Eng.* **111**, 248–255 (1989)

7 Lin, C. A. and Tsai, J. H. Computations of strongly swirling flow with second-moment closure, *16th National Conf. on Theoretical and Applied Mechanics*, 11–12 December, Keelung, Taiwan, 127–134 (1992)

8 Jones, W. P. and Launder, B. E. The prediction of laminarisation with a two-equation model of turbulence, *Int. J. Heat Mass Transfer*, Vol. 15, pp. 301–314 (1972)

9 Gibson, M. M. and Launder, B. E. Ground effects on pressure fluctuations in the atmospheric boundary layer, *J. of Fluid Mechanics*, **86**, 491–511 (1978)

10 Lin, C. A. and Leschziner, M. A. Three-dimensional computation of transient interaction between radially injected jet and swirling cross-flow using second-moment closure, *Proc. 4th Int. Symp. on Computational Fluid Dynamics*, pp. 686–692 (1991)

11 Patankar, S. V. and Spalding, D. B. A calculation procedure for heat, mass and momentum transfer in three-dimensional parabolic flows, *Int. J. Heat Mass Transfer*, **15**, 1787–1806 (1972)
12 Leonard, B. P. A stable and accurate convective modelling procedure based on quadratic upstream interpolation, *Comp. Meth. Appl. Mech. Eng.*, **19**, 59–98 (1979)
13 Favaloro, S. C., Nejad, A. S. and Ahmed, S. A. Experimental and computational investigation of isothermal swirling flow in an axisymmetric dump combustor, *J. Propulsion*, **7**, 3, 348–356 (1991)
14 Launder, B. E. *Low-Reynolds Number Turbulence Near Walls*, Rep. TFD/86/4, Dept. of Mech. Eng., UMIST, Manchester, UK (1986)